Autonomous Driving in 5G: Mitigating Interference in OFDM-Based Vehicular Communications

Evangelos Vlachos[1], Aris S. Lalos[2], Kostas Berberidis[1] and Christos Tselios[2]

[1] Dept. of Computer Engineering and Informatics, University of Patras & C.T.I, Greece
{vlaxose,berberid}@ceid.upatras.gr
[2] Dept. of Electrical and Computer Engineering, University of Patras, Greece
{aris.lalos, tselios}@ece.upatras.gr

***Abstract*—Automotive industry will be greatly benefited by the advent of 5G Networking and the huge boost in performance and coverage it will support. Road safety and traffic efficiency services will be significantly upgraded through seamlessly interconnected devices, while latency decrease will most likely allow autonomous driving to become a commodity, available to everyone. This technology will have a huge societal and economical impact, since it will render severe traffic accidents, long commute times and increased energy consumption obsolete. Current vehicular communication systems are usually equipped with orthogonal frequency division multiplexing (OFDM) transceivers that operate in suboptimal modes for the upcoming 5G standards. The problem originates in the existing intercarrier interference (ICI) on the receiver end, often partially tackled by integrated successive interference cancellation (OSIC) architectures. However, for decreasing complexity, system designers attempt to mitigate ICI by considering only a small number or sub-carriers, leading to error floor introduction and unacceptable bit-error-rates (BER). This paper presents an OSIC-based solution for cancelling interference in OFDM systems operating over specific conditions such as doubly selective channels. The experimental results indicated that the proposed equalizer outperforms all existing non-banded ICI cancellation methods, by achieving lower BER despite operating in a resource-savvy manner.**

***Index Terms*—OFDM, ICI, OSIC, ADV, V2X, 5G.**

I. Introduction

The advent of the 5G Networking era introduces novel, fascinating verticals that will probably influence our everyday lives harsher than any other cellular network architecture modification. The expected interconnected device increase and the user-oriented demand for seamless connectivity and ultra-high-speed data transfer will lead to a holistic re-design of telecommunication networks. Certain benefits of a commercial network supporting more than 10 billion interconnected cellular devices [1], operating with less than 1 ms end to end latency, 99.99% availability and up to a thousand times larger throughput [2], will become apparent when new applications emerge and influence factors ranging from entertainment to private transportation [3],[4].

The automotive domain has always been divided into two distinct yet correlated tracks, autonomous driving vehicles (ADV) and vehicle-to-everything (V2X) communication. The arrival of 5G is expected to tackle the major challenging issues of autonomous driving, namely (i) the exact vehicle position retrieval (ii) the identification of the actual surrounding environment conditions for collision avoidance (iii) the traffic sign and road condition identification (i.e. lanes, signs, light signals and tarmac status) [5]. Through advanced V2X solutions, an ADV will be rendered capable of interacting with other vehicles which support collision avoidance safety systems (V2Vehicle), identify traffic signal timing or priority (V2Infrastructure), obtain traffic information or routing guidance in real-time over the cloud (V2Network) and provide safety alerts to pedestrians (V2Pedestrian). This disruptive technology will have a significant economic and societal impact, due to the decrease of driving accidents and the more predictable and productive commute time [6].

As shown in Fig.1, V2X is a key technology enabler for autonomous driving by allowing vehicles to safely drive in shorter distances to each other, thus enabling traffic flow optimization solutions. In addition, V2X offers increased situational awareness since it has the ability of gathering data a-priori and analyze them to deliver a more predictable driving experience. Such data may include status information (i.e. vehicle speed, status, acceleration) or event information (i.e. traffic jam, icy road, accident notification), being disseminated to neighboring vehicles over the V2V interface, or submitted to a centralized database for further process before being distributed to the network. According to [7] the next evolutionary step will be to engage the vehicles on-board sensors, create data stream groups originating from nearby sources and provide enhanced information in real-time to all moving vehicles. This will render drivers capable of responding properly to blind intersections, avoiding collisions in closed curves or during lane switching and overtaking cases, discover available parking spots and generally drive safely in an environment where traffic signal priority, maximum speed limits and adaptive cruise control and platooning are centrally enforced.

One of the biggest issues that 5G must solve is backwards compatibility with existing infrastructure and available user equipment. Especially during the first years of its deployment, until all links of the value chain come in sync, 5G solutions need to ensure that previous generation devices are supported and provide the means for them to reach certain standards of functionality and speed. This is the primal reason that

current generation networking solutions based on 3GPP Long Term Evolution (LTE) or IEEE 802.11p also need to evolve, thus being able to be integrated in the upcoming ecosystem seamlessly and with the greatest of ease ensuring a certain level of end-user Quality of Experience (QoE).

The original design of LTE was made with the use case of mobile broadband traffic in mind. This is the apparent reason of certain limitation this architecture has when it comes to V2X communication. In cellular transmission a central networking entity grants transmission rights upon request. This centralized approach may minimize interference and allow optimal collision avoidance, but also leads to bottlenecks since every data packet must traverse the infrastructure through uplink and downlink transmissions. Latency rises when more users are located in the same cell and last but not least, out of coverage functionality (i.e. tunnels, rural areas, underground passages) is simply not an option. On the other hand, the IEEE 802.11p offers direct communication channel between source and destination endpoints and is able to operate in a distributed fashion even without network infrastructure coverage, but in cases where network load increases performance quickly degrades. The root cause of this behavior is traced to the contention-based medium access strategy, which follows the listen before talk principle. The higher the number of devices transmitting in a certain area, the higher the possibility of a device to postpone its transmission as the result of the occupied channel. Possible re-transmissions further increase latency, therefore a maximum latency is impossible to be estimated.

Given the fact that each V2X communication solutions has specific pros and cons, most researchers decide to provide solutions at a lower level and investigate a widely employed data communication technique, the orthogonal frequency division multiplexing (OFDM). OFDM systems divide the entire communication channel into narrow orthogonal subchannels, thus achieving the elimination of intersymbol interference (ISI) originally introduced by underlying multipath environments.

However, since mmWave communication systems operate in considerably increased frequency bands will experience severe intercarrier interference (ICI) in the receiver, since the temporal variations within a single OFDM block corrupt the orthogonality of the subchannel and generate power leakage. This limitation not only poses a threat to 5G's proclaimed functionality in ultra-dense environments but also motivated system architects to focus on alternative equalization mechanisms for mitigating ICI in an effective manner.

OFDM cannot be replaced overnight, since it has been adopted by popular telecommunication platforms that define an over-the-air interface between a wireless client and a base station or between two wireless clients, along with the dominant cellular telecommunications standard LTE / LTE-A. Nevertheless, low complexity and computational ease is always appreciated for any potential solution.

The performance of linear equalization schemes seems to be unacceptable in systems that experience severe ICI [8]. To deal efficiently with this effects more complex solutions are required, that usu sally become in feasible is systems with a large number of sub-carriers. For tackling this limitation some researchers reside on using banded equalization schemes [9],[10], which appear to be quite attractive due to their simplicity, alas significantly degrades when high mobility scenarios are investigated. Motivated by all aforementioned issues, we focus on the non-banded schemes, and we propose an ordered successive interference cancellation architecture that selects at each stage a seed equalizer and estimates the respective coefficients using the conjugate gradient method. The non seed equalizers are estimated by using Galerking projections and the resulting coefficients are then used for the selection of the following seed equalizer that will be used for detecting the symbol that is transmitted at the respective sub-carrier of the following stage. The complexity of the proposed techniques heavily depends on the termination parameter and can even be an order of magnitude smaller than the conventional OSIC approach without affecting noticeably the performance.

The rest of the paper is organized as follows: the OFDM architecture together with the actual problem formulation can be found in Section II, while the equalization scheme is analyzed in Section III. Simulation results are shown in Section IV and last but not least, Section V summarizes the conclusions of this work.

II. OFDM Architecture & System Model

Let us consider an OFDM system with N sub-carriers operating over a doubly selective channel. Let $\mathbf{s} = [\ s_1 \quad \dots \quad s_N\ ]^T \in \mathbb{C}^{N\times 1}$ be a set of N symbols at the output of the Constellation Mapper that are forwarded to the input of the OFDM Modulator. The s_k symbol is transmitted via the k-th sub-carrier. The output of the Inverse Discrete Fourier Transform (IDFT) unit, denoted by $\mathbf{u} \triangleq \mathbf{F}^H\mathbf{s} \in \mathbb{C}^{N\times 1}$, is forwarded at the Cyclic Prefix (CP) Adder, where the OFDM symbol $\hat{\mathbf{u}} \in \mathbb{C}^{M\times 1}$ of length $M = N + N_{cp}$ is formed by adding a CP of length N_{cp}. In mathematical terms the CP addition can be written as $\hat{\mathbf{u}} \triangleq \mathbf{C}^{cp}\mathbf{s}$ where:

$$\mathbf{C}^{cp} = \begin{bmatrix} \mathbf{0}_{N_{cp}\times(N-N_{cp})} & \mathbf{I}_{N_{cp}} \\ & \mathbf{I}_N \end{bmatrix}. \tag{1}$$

The doubly selective channel is modeled as a Wide Sense Stationary Uncorrelated Scattering (WSSUS) channel [11] and the channel impulse response (CIR) of this WSSUS channel is expressed as $h(n,\tau) = \sum_{l=0}^{L-1} a(n,l)\delta(\tau - l)$, where $a(n,l)$ is complex zero mean Gaussian random variable. Assuming a causal channel with maximum delay spread $L \leq N_{cp}$, the received signal at the input of the OFDM de-modulator is given by:

$$\mathbf{x} \triangleq \tilde{\mathbf{H}}_t\hat{\mathbf{u}} + \hat{\mathbf{w}} \tag{2}$$

where $\tilde{\mathbf{H}}_t \in \mathbb{C}^{M\times M}$ with $[\tilde{H}_t]_{i,j} = a\big(i, mod(i-j, L)\big)$ with $i,j \in 1,\dots,M$, while $mod(\cdot, L)$ denotes the modulo-L the operation. The vector $\hat{\mathbf{w}} \in \mathbb{C}^{M\times 1}$ represents the white Gaussian noise (AWGN) with $\hat{\mathbf{w}} \sim \mathcal{N}(0, \sigma^2\mathbf{I}_M)$. The output of the OFDM de-modulator after ignoring potential sampling and carrier frequency offsets can be written as:

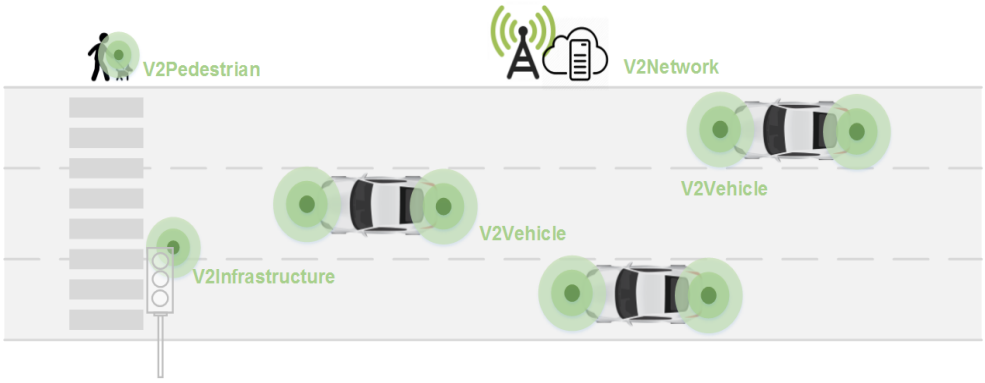

Fig. 1: Autonomous Driving in the 5G Networking Era

$$\mathbf{y} \triangleq \mathbf{Fz} = \underbrace{\mathbf{F}\mathbf{R}^{cp}\tilde{\mathbf{H}}_t\mathbf{C}^{cp}\mathbf{F}^H}_{\mathbf{H}}\mathbf{s} + \mathbf{w} = \mathbf{Hs} + \mathbf{w} \tag{3}$$

where, the operator $\mathbf{R}^{cp}$ discards the N_{cp} samples of the CP. At this point, it should be also noted that the entries of $\mathbf{w}$ are also complex normal RVs with zero mean and variance σ^2.

In the time-invariant case, matrix $\tilde{\mathbf{H}}_t$ has a Toeplitz structure, i.e. $a_i(1) = a_i(2) = \cdots = a_i(N)$, $i = 1, \ldots L$, and thus matrix $\mathbf{H}$ becomes diagonal since matrix $\mathbf{R}^{cp}\tilde{\mathbf{H}}_t\mathbf{C}^{cp}$ is circulant, and therefore the equalization in the FD requires $\mathcal{O}(N)$ complex floating point operations. In the time-varying case, matrix $\mathbf{H}$ is no longer diagonal and more complex equalization schemes are required.

III. Proposed Equalization scheme

One of the most common approaches that are adopted in the time- and frequency- selective cases are equalization schemes that are based in the OSIC architecture. These schemes offer significant performance benefits as compared to the linear approaches requiring though, higher complexity. In this section, we describe the proposed ordered successive interference cancellation schemes that employ a well known linear algebra method for solving linear systems with multiple RHSs, known as Galerkin projections (GPs). We initially formulated the problem of estimating the equalizer for sub-carrier k as a problem of solving multiple linear systems and then we exploit coherences between different systems using the GPs. More specifically, one system is selected as 'seed' and is solved using Conjugate Gradient (CG) iterations, while the other systems update their solutions by performing Galerkin Projections. The seed selection is determined by the ordering mechanism that is applied at each stage. The basic steps of the proposed architecture at each stage k are the: i) evaluation of the seed equalizer coefficient using CG ii) evaluation of the non seed equalizer coefficients using GP iii) Ordering and identification of the system that will be selected as seed in the next stage. Each one of these steps is presented in the rest part of this section.

A. Evaluating 'Seed' Equalizer

After taking into account that the N data symbols are transmitted via N sub-carriers, the interference cancelation is performed in N *stages*, where at each stage we subtract the part of the ICI which is associated with the decisions already made at previous stages. Specifically, assuming that the symbols are detected sequentially, i.e., $s_{z_1}, s_{z_2}, \ldots, s_{z_N}$, then at each stage, we estimate the equalizer that minimizes the minimum-mean-square error (MMSE) criterion, expressed as:

$$\mathbf{g}_{z_k} = arg\min_{\mathbf{g}_{z_k}} \frac{1}{2}\mathcal{E}\{|\mathbf{g}_{z_k}^H\mathbf{y}_{z_k} - s_{z_k}|^2\}, \;\; k = 1, \ldots, N \tag{4}$$

where $\mathbf{g}_{z_k}$ denotes the filter that cancels the interference introduced in the k sub-carrier, and $\mathbf{y}_{z_k}$ is the updated vector of the time domain symbols at the receiver after the cancellation of $k-1$ previously detected symbols, with $\mathbf{y}_{z_1} \triangleq \mathbf{y}$.

Equivalently, the minimizer of the aforementioned cost function can be calculated as the solution of the following linear system, so called as 'seed' system:

$$\left(\mathbf{H}_{z_k}^H\mathbf{H}_{z_k} + \sigma^2\mathbf{I}_{N-k+1}\right)\mathbf{g}_{z_k} = \mathbf{h}_{z_k} \tag{5}$$

where $\mathbf{h}_{z_k}$ is the z_k-th column of the channel matrix $\mathbf{H}_{z_k}^H$, and $\mathbf{H}_{z_k}$ denotes the channel matrix after the removal of the $k-1$ columns $\{\mathbf{h}_{z_1}, \ldots, \mathbf{h}_{z_{k-1}}\}$, with $\mathbf{H}_{z_1} \triangleq \mathbf{H}$. The solution of the seed system can be efficiently estimated by using the Conjugate Gradient (CG) method, that sequentially updates the solution $\mathbf{g}_m^i$ by performing steps in $\mathbf{A}_{z_k}$ - orthogonal directions, where $\mathbf{A}_{z_k} \triangleq \left(\mathbf{H}_{z_k}^H\mathbf{H}_{z_k} + \sigma^2\mathbf{I}_{N-k+1}\right)$. At the i-th CG iteration, the basis of the Krylov subspace $\mathcal{K}_{m,i} = span\{\mathbf{d}_m^0, \mathbf{d}_m^1, \ldots, \mathbf{d}_m^{i-1}\}$ determines the search space where the approximated solution lies and $\mathbf{d}_m^\ell$ is the search direction of the m-th system at the ℓ-th iteration. After at most N iterations, the obtained solution $\mathbf{g}_m \triangleq \mathbf{g}_m^N$, are the minimizers of the following quadratic cost function $\mathcal{J}$, i.e.

$$\mathcal{J}(\mathbf{g}_m) = \frac{1}{2}\mathbf{g}_m^H\mathbf{A}_{z_k}\mathbf{g}_k - \mathbf{h}_m^H\mathbf{g}_m. \tag{6}$$

The search direction $\mathbf{d}_m^i$ in the i-th step is constructed by applying the Gram-Schmidt procedure to the residual vectors $\mathbf{r}_m^i = -\nabla\mathcal{J}(\mathbf{g}_m^i) = \mathbf{h}_m - \mathbf{A}_{z_k}\mathbf{g}_m^i$ and the preceding

directions $\mathbf{d}_m^0, \mathbf{d}_m^1, \ldots, \mathbf{d}_m^{i-1}$. By exploiting the orthogonality of the gradient $\nabla\mathcal{J}(\mathbf{g}_m^i)$ to the previous direction vectors, we end up at the following updating rule:

$$\mathbf{d}_m^i = \mathbf{r}_m^i + \beta^i \mathbf{d}_m^{i-1} \tag{7}$$

where $\beta^i = \frac{(\mathbf{r}_m^i)^H \mathbf{r}_m^i}{(\mathbf{r}_m^{i-1})^H \mathbf{r}_m^{i-1}}$. For the given set of i $\mathbf{A}$-conjugate directions, the approximate solution $\mathbf{g}_m^i$ can be expressed as follows:

$$\mathbf{g}_m^i = \alpha^0 \mathbf{d}_m^0 + \ldots + \alpha^i \mathbf{d}_m^i = \mathbf{x}_m^{i-1} + \alpha^i \mathbf{d}_m^i \tag{8}$$

where the scalar value α^i is obtained as the minimizing argument of the quadratic function with respect to α^i, i.e., $\alpha^i = \frac{(\mathbf{r}_m^i)^H \mathbf{r}_m^i}{(\mathbf{d}_m^i)^H \mathbf{A}_{z_k} \mathbf{d}_m^i}$. The residual vector at the i-th iteration can be updated according to $\mathbf{r}_m^i = \mathbf{r}_m^{i-1} - \alpha^i \mathbf{A}_{z_k} \mathbf{d}_m^i$.

After the termination of the iterative algorithm, the estimated solution of (5), is used to detect the current symbol as:

$$\hat{s}_{z_k} = \Pi(\mathbf{g}_{z_k}^H \mathbf{y}_{z_k}). \tag{9}$$

The decision $\hat{s}_{z_k}$ is then used for estimating the respective ICI, that is $\mathbf{h}_{z_k}\hat{s}_{z_k}$, which is then subtracted by the following received symbol $y_{z_{k+1}}$, i.e.

$$\mathbf{y}_{z_{k+1}} = \mathbf{y}_{z_k} - \mathbf{h}_{z_k}\hat{s}_{z_k} \tag{10}$$

and the aforementioned procedure is repeated for the detection of $s_{z_{k+1}}$.

B. Ordering and Evaluation of the 'Non Seed' Equalizers

The performance of an OSIC scheme is significantly affected by the detection order of the symbols transmitted to the following sub-carriers [12], [13]. The most common criterion for obtaining the optimal detection order is the maximization of the signal-to-interference and noise power ratio (SINR) at the receiver, that corresponds to the minimization of the achievable bit error rate (BER) at the output of the OFDM demodulator. In mathematical terms, at each stage k, this maximization can be written as:

$$\mathrm{z}_k = arg\max_{l} \frac{|\mathbf{g}_l^H \mathbf{h}_l|^2}{\sum\limits_{\substack{m \\ m \neq k}} |\mathbf{g}_l^H \mathbf{h}_m|^2 + \sigma\|\mathbf{g}_l\|_2^2}, \quad \forall l \in [z_{k+1}, z_{k+2}, \ldots, z_N]. \tag{11}$$

Thus, the SINR calculation at the stage z_k, requires the estimation of $\mathbf{g}_{z_{k+1}}, \ldots, \mathbf{g}_{z_N}$ equalization vectors, which are estimated by solving the following systems of linear equations:

$$\mathbf{A}_{z_k}\mathbf{g}_l = \mathbf{h}_l, \text{ with } l \in [z_{k+1}, z_N] \tag{12}$$

where the auto-correlation matrix is the same for all the systemsin each stage.

The approximate solutions of the remaining $N-1$ non-seed systems, i.e.,

$$\mathbf{A}_{z_k}\mathbf{g}_l = \mathbf{h}_l^H, \text{ with } l \in [2, \ldots, N] \tag{13}$$

are obtained as the solution of the following optimization problems $\min_\alpha \mathcal{J}(\mathbf{g}_l^i + \alpha \mathbf{d}_m^i)$ for all l. Thus the remaining equalization vectors can be updated by:

$$\mathbf{g}_l^i = \mathbf{g}_l^{i-1} + \alpha^l \mathbf{d}_m^i \tag{14}$$

where $\alpha^l = \frac{(\mathbf{d}_m^i)^H \mathbf{r}_l^{i-1}}{(\mathbf{d}_m^i)^H \mathbf{A}_{z_k}^H \mathbf{d}_m^i}$ and $\mathbf{r}_l^{i-1}$ is estimated by:

$$\mathbf{r}_l^i = \mathbf{r}_l^{i-1} - \alpha^l \mathbf{A}_{z_k}^H \mathbf{d}_m^i. \tag{15}$$

Finally, it is important to note that the matrix vector product $\mathbf{A}_{z_k}^H \mathbf{d}_m^i$ has been computed during the execution of the i-th CG iteration of the seed linear system. The aforementioned steps are summarized in the table that follows. More specifically, the "for" loop at line 2, represents the stages, while the termination condition is evaluated at line 4. The seed equalizers are estimated at lines 5-16, while the non seed ICI cancellation filters are approximated at lines 17-21. The computational demanding tasks of the algorithm are the matrix-vector products in lines 12 and 18.

Algorithm 1: Proposed ICI cancellation approach

Data: $\mathbf{A}_{z_k}$, $\mathbf{H}_{z_k}$, $\mathbf{G}^0$
Result: $\mathbf{G}$

1 Initialization: $\mathbf{R}^0 = \mathbf{H}_{z_k} - \mathbf{A}_{z_k}\mathbf{G}^0$
2 **for** $m = 1, 2, \ldots, N-k+1$ **do**
3 $i \longleftarrow 0$
4 **while** $\|\mathbf{r}_m^{i-1}\| < \epsilon$ **do**
5 $\rho^i \longleftarrow \|\mathbf{r}_m^{i-1}\|$
6 **if** $i = 0$ **then**
7 $\mathbf{d}_m^i \longleftarrow \mathbf{r}_m^{i-1}$
8 **else**
9 $\beta^i \longleftarrow \rho^i / \rho^{i-1}$
10 $\mathbf{d}_m^i \longleftarrow \mathbf{r}_m^{i-1} + \beta^i \mathbf{d}_m^{i-1}$
11 $\boldsymbol{\mathcal{V}}^i \longleftarrow \mathbf{A}_{z_k}\mathbf{d}_m^i$
12 $\mathcal{C}^i \longleftarrow (\mathbf{d}_m^i)^H \boldsymbol{\mathcal{V}}^i$
13 $\alpha^i \longleftarrow \rho^i / \mathcal{C}^i$
14 $\mathbf{g}_m^i \longleftarrow \mathbf{g}_m^{i-1} + \alpha^i \mathbf{d}_m^i$
15 $\mathbf{r}_m^i \longleftarrow \mathbf{r}_m^{i-1} - \alpha^i \boldsymbol{\mathcal{V}}^i$
16 **for** $\ell = m+1, \ldots, N$ **do**
17 $\zeta^i \longleftarrow (\mathbf{d}_m^i)^H \mathbf{r}_\ell^{i-1} / \mathcal{C}^i$
18 $\mathbf{g}_\ell^i \longleftarrow \mathbf{g}_\ell^{i-1} + \zeta^i \mathbf{d}_m^i$
19 $\mathbf{r}_\ell^i \longleftarrow \mathbf{r}_\ell^{i-1} - \zeta^i \boldsymbol{\mathcal{V}}^i$
20 $i \longleftarrow i+1$

Performance/Complexity Trade-off: The termination of Algorithm 1 is determined by the absolute norm of the residual vector. The threshold value ϵ has a direct impact on the number of required iterations for convergence and determines both the performance and the complexity of the proposed approach. It can be easily shown that there is a strong relation between the parameter ϵ and the reconstruction error of the algorithm, defined as $\zeta \triangleq \|\mathbf{g}_m^\star - \mathbf{g}_m^I\|$.

TABLE I: Fundamental parameters used in simulation experiments

Parameter	Value
Modulation mode	4QAM, 16QAM
Subcarrier	$N = 32$
FFT length	32
Channel length	$L = 3$
Cyclic prefix length	$N_{cp} = 3$

If we denote with I the executed iteration for the m system, the error residual can be written as:

$$\mathbf{r}_m^I = \mathbf{b}_m - \mathbf{R}_m \mathbf{g}_m^I = \mathbf{A}_{z_k} \mathbf{g}_m^\star - \mathbf{A}_{z_k} \mathbf{g}_m^I = \mathbf{A}_{z_k} \left(\mathbf{g}_m^\star - \mathbf{g}_m^I \right) \tag{16}$$

where $\mathbf{g}_m^\star$ denotes the interference cancellation filter computed in (5). Then, the norm of the error is bounded as follows:

$$\|\mathbf{r}_m^I\| < \|\mathbf{A}_{z_k}\| \|\mathbf{g}_m^\star - \mathbf{g}_m^I\| = \|\mathbf{A}_{z_k}\| \zeta \tag{17}$$

To proceed, note that $\|\mathbf{A}_{z_k}\| = \|\mathbf{H}_{z_k}^H \mathbf{H}_{z_k} + \sigma^2 \mathbf{I}\| < \|\mathbf{H}_{z_k}^H \mathbf{H}_{z_k}\| + \sigma^2 < \|\mathbf{H}_{z_k}\|^2 + \sigma^2$. Since $\mathbf{H}_{z_k}$ has $k-1$ fewer columns than $\mathbf{H}_{z_1}$, we have that $\|\mathbf{H}_{z_k}\| < \|\mathbf{H}\|$, hence we have that $\|\mathbf{A}_{z_k}\| < \|\mathbf{H}\|^2 + \sigma^2$. Therefore, the residual error is upper bounded by:

$$\|\mathbf{r}_m^I\| < \left(\|\mathbf{H}\|^2 + \sigma^2 \right) \zeta \triangleq \epsilon \tag{18}$$

i.e. ϵ correspond to the normalized error and Eq. (18) represents the termination condition. A small value for the threshold would result into small reconstruction error increasing significantly the number of iterations ($I \to N$), which are required in order to reach the desired accuracy. On the other hand, a large threshold value decreases both the accuracy and the number of required iterations ($I \ll N$).

IV. Simulation Results

This section includes the proposed equalizer performance evaluation through extensive simulation. All parameters were selected in line with the IEEE 802.11p standard. In addition, full channel state information at the receiver was assumed, together with perfect carrier and phase synchronization in all participating entities.

A. Setup

The overall setup revolves around an OFDM system simulation, operating over a doubly selective channel. Table I presents the fundamental parameters used in the particular set of simulation experiments. In regards to channel modeling, the wide-sense stationary uncorrelated scattering (WSSUS) fading model was adopted, with a 3-tap exponential delay power profile, as indicated by:

$$\sigma_h^2(l) = \frac{e^{-l/L}}{\sum_{m=0}^{L-1} e^{-m/L}}, \text{ for } l = 0, 1, \dots L-1 \tag{19}$$

where $L = 3$. Jakes' model [14] was utilized to generate the Doppler spectrum of the complex Gaussian random process independently used for each channel tap, while the autocorrelation function of each channel tap is equal to the zeroth order Bessel function of the first kind, i.e. $r_t(\Delta t) = J_0(2\pi f_d \Delta t)$, where $\Delta t \in [-N, N] \subset \mathbb{Z}$, with f_d being the normalized Doppler spread defined as $f_d \triangleq \frac{1}{F} \frac{f_c v}{c}$. In the previous equation, v is the relative velocity of the vehicle, f_c corresponds to the carrier frequency, F portrays the subcarrier separation, while c is the speed of light. Throughout our simulated experimentation, we have ratified the normalization over the signaling rate [10], for instance $F = N$.

For properly evaluating the proposed equalizer's performance, it is essential to compare it with numerous similar approaches conducted over the last few years. In particular, we have focused on: i) the equalizer presented in [15] (termed as *Block OSIC, non-banded*), while ii) the used the equalizer proposed in [16] (termed as *Block MMSE, banded-windowed*) was used as a low complexity technique.

Soft decisions in all banded equalization schemes are calculated using the following formula:

$$\tilde{\mathbf{x}}_{\mathbf{w}} = \mathbf{H}_K^H \left(\mathbf{H}_K \mathbf{H}_K^H + \frac{\sigma_z^2}{\gamma} \mathcal{C}(\mathbf{w}) \mathcal{C}(\mathbf{w})^H \right)^{-1} \mathbf{y}_{\mathbf{w}} \tag{20}$$

where $\mathbf{H}_K$ translates as the K-banded approximation of the frequency-domain channel matrix, The parameter $\gamma \in (0, 1]$ acts as the regularization parameter, while $\mathbf{w}$ corresponds to the received symbol's $\mathbf{y}$ applied window, with $\mathbf{y}_{\mathbf{w}} \triangleq \mathcal{C}(\mathbf{w})\mathbf{y}$. In addition, the maximum SINR criterion [10] was used for the aforementioned window design.

Additionally, the serial equalizer introduced by [17] (termed as *Serial DFE*) was used as an alternative to block equalization. The overall sub-carriers number processed at each step equals to K. Another decisive factor of the technique in [17] is the PIC operation, applied to the equalizer's output. The actual number of PIC iterations determines the overall trade-off of the proposed technique in terms of both complexity and performance.

B. BER performance

Figure 2 presents the BER of 4QAM modulation w.r.t. SNR, for numerous distinct values of normalized Doppler frequency f_d. It is rather obvious that, for medium Doppler spreads ($f_d = 0.05$), there is no prevailing technique in terms of absolute performance. When it comes to higher Doppler spreads, both banded and serial approximation techniques suffer from severe ICI, while any change in the value of K is directly linked to a significant performance deterioration. For $f_d = 0.3$ the BER performance of block DFE technique [18] is parallel to the OSIC one, however for higher Doppler spreads, an increase to the K value is necessary for the system to retain this performance. On the contrary, the OSIC techniques demonstrate a profound ability towards effectively mitigating ICI regardless of the Doppler spread on each case. Results show that the proposed technique's BER closely approximates that of the non-banded block OSIC equalizer [15], only depending on the parameter ϵ.

V. Conclusion

The automotive industry is currently experiencing a rapid technological transformation phase. Modern vehicles are

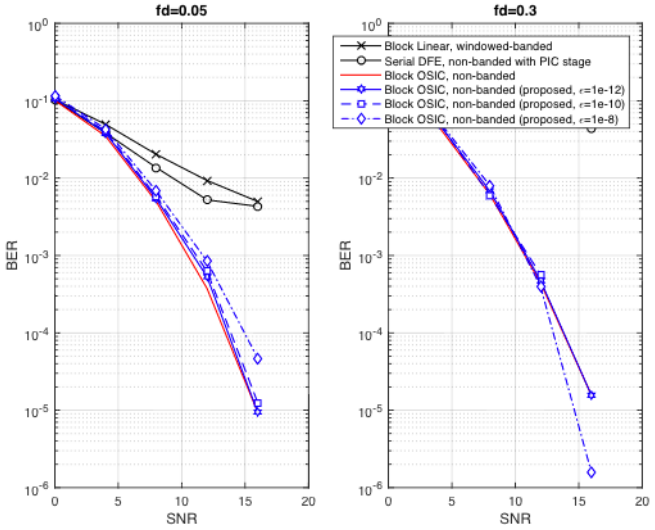

Fig. 2: BER comparison w.r.t. SNR for medium and high Doppler spread and 4QAM

equipped with novel communication systems that allow connectivity not only to the network infrastructure, but to any neighboring device with compatible interfaces. This trend is likely to escalate in the near future when 5G, the next generation of mobile communication arrives. However, it is necessary to ensure backwards compatibility with currently deployed devices, therefore existing technologies also need to evolve. In this paper, we have presented an OSIC-based solution for cancelling interference in OFDM systems. Equalizer filters were efficiently estimated through a CG-based mechanism. This mechanism utilizes Galerkin projections for initializing filters, thus vastly accelerating the algorithm's convergence rate. The outcome of our experiments indicated that the proposed equalizer outperforms all commonly used non-banded ICI cancellation methods, by achieving less BER despite operating in a resource-savvy manner. Our solution aims to render existing V2X communication platforms more agile and trustworthy, thus allowing their integration to the novel framework that briskly approaches.

REFERENCES

[1] Ericsson, "Mobility Report, June 2016," Available: https://www.ericsson.com/res/docs/2016/ericsson-mobility-report-2016.pdf, [Online].

[2] C. Tselios and G. Tsolis, "On QoE-awareness through Virtualized Probes in 5G Networks," in *Computer Aided Modeling and Design of Communication Links and Networks (CAMAD), 2016 IEEE 21st International Workshop on*, 2016, pp. 1–5.

[3] G. Bianchi, E. Biton, N. Blefari-Melazzi *et al.*, "Superfluidity: a flexible functional architecture for 5g networks," *Transactions on Emerging Telecommunications Technologies*, vol. 27, no. 9, pp. 1178–1186, 2016.

[4] C. Tselios and G. Tsolis, "A survey on software tools and architectures for deploying multimedia-aware cloud applications," in *Lecture Notes in Computer Science: Algorithmic Aspects of Cloud Computing*. Springer International Publishing, 2016, vol. 9511, pp. 168–180.

[5] J. Choi, J. Lee, D. Kim, G. Soprani, P. Cerri, A. Broggi, and K. Yi, "Environment-detection-and-mapping algorithm for autonomous driving in rural or off-road environment," *IEEE Transactions on Intelligent Transportation Systems*, vol. 13, no. 2, pp. 974–982, June 2012.

[6] L. Hobert, A. Festag, I. Llatser, L. Altomare, F. Visintainer, and A. Kovacs, "Enhancements of v2x communication in support of cooperative autonomous driving," *IEEE Communications Magazine*, vol. 53, no. 12, pp. 64–70, Dec 2015.

[7] The 5G-PPP, "5G-PPP White Paper on Automotive Vertical Sector," Available: https://5g-ppp.eu/wp-content/uploads/2014/02/5G-PPP-White_Paper-on-Energy-Vertical-Sector.pdf, [Online].

[8] E. Vlachos, A. S. Lalos, and K. Berberidis, "Regularized mmse ici equalization for ofdm systems over doubly selective channels," in *IEEE International Symposium on Signal Processing and Information Technology*, Dec 2013, pp. 000 458–000 463.

[9] ——, "Low-complexity osic equalization for ofdm-based vehicular communications," *IEEE Transactions on Vehicular Technology*, vol. 66, no. 5, pp. 3765–3776, May 2017.

[10] P. Schniter, "Low-complexity equalization of ofdm in doubly selective channels," *IEEE Transactions on Signal Processing*, vol. 52, no. 4, pp. 1002–1011, April 2004.

[11] P. Bello, "Characterization of randomly time-variant linear channels," *IEEE Transactions on Communications Systems*, vol. 11, no. 4, pp. 360–393, December 1963.

[12] P. W. Wolniansky, G. J. Foschini, G. D. Golden, and R. A. Valenzuela, "V-blast: an architecture for realizing very high data rates over the rich-scattering wireless channel," in *1998 URSI International Symposium on Signals, Systems, and Electronics. Conference Proceedings (Cat. No.98EX167)*, Sep 1998, pp. 295–300.

[13] A. Lozano and C. Papadias, "Layered space-time receivers for frequency-selective wireless channels," *IEEE Transactions on Communications*, vol. 50, no. 1, pp. 65–73, Jan 2002.

[14] W. C. Jakes and D. C. Cox, Eds., *Microwave Mobile Communications*. Wiley-IEEE Press, 1994.

[15] Y.-S. Choi, P. J. Voltz, and F. A. Cassara, "On channel estimation and detection for multicarrier signals in fast and selective rayleigh fading channels," *IEEE Transactions on Communications*, vol. 49, no. 8, pp. 1375–1387, Aug 2001.

[16] L. Rugini, P. Banelli, and G. Leus, "Low-complexity banded equalizers for ofdm systems in doppler spread channels," *EURASIP Journal on Advances in Signal Processing*, vol. 2006, no. 1, p. 067404, 2006. [Online]. Available: http://dx.doi.org/10.1155/ASP/2006/67404

[17] X. Cai and G. B. Giannakis, "Bounding performance and suppressing intercarrier interference in wireless mobile ofdm," *IEEE Transactions on Communications*, vol. 51, no. 12, pp. 2047–2056, Dec 2003.

[18] L. Rugini and P. Banelli, "Performance analysis of banded equalizers for ofdm systems in time-varying channels," in *2007 IEEE 8th Workshop on Signal Processing Advances in Wireless Communications*, June 2007, pp. 1–5.